Thermodynamic modeling of the Mo–Pt system based on the NACEF approach

J.M. Fiorani, M. Siblani, J. -M. Joubert, C. Barreteau, J.-C. Crivello, Nicolas David, M. Vilasi

Thermodynamic modeling of the Mo–Pt system based on the NACEF approach

J.-M. Fiorani [(a)], M. Siblani [(a)], J.-M. Joubert [(b)], C. Barreteau [(b)], J.-C. Crivello [(c)], N. David [(a)], M. Vilasi [(a)]

[a] Univ. de Lorraine, CNRS, Institut Jean Lamour, UMR 7198, Campus ARTEM, 2 allée André Guinier, 54011 Nancy, France

[b] Univ. Paris Est Créteil, CNRS, ICMPE, UMR 7182, 2 rue Henri Dunant, 94320 Thiais, France

[c] Current address: CNRS - Saint-Gobain - NIMS, IRL 3629, Laboratory for Innovative Key Materials and Structures (LINK), 305-0044 Tsukuba, Japan

Keywords:
Thermodynamic modeling
Mo–Pt
CALPHAD
New Approach to the Compound Energy Formalism (NACEF)
Order/Disorder transitions
Ab initio calculations

ABSTRACT

The present work reports on a thermodynamic modeling of the Mo–Pt system using a combined first-principles/CALPHAD approach. First-Principles (FP) calculations are performed to obtain the enthalpies of formation for the four ordered phases of the system (*A*15, *B*19, $D0_{19}$ and $MoPt_2$) at 0 K. The liquid, bcc, fcc and hcp phases have been modeled as substitutional solutions where the excess term is in the form of the Redlich–Kister polynomial. The four ordered phases are modeled using the NACEF approach taking into account the three order-disorder transitions (*B*19/*A*3, $D0_{19}$/*A*3 and $MoPt_2$/*A*1). FP calculations, experimental phase equilibria and site occupancies data are used to evaluate the model parameters. The thermodynamic description of the Mo–Pt system obtained in this work agree well with all the available data with a limited number of parameters used.

1. Introduction

Due to their good properties such their oxidation and corrosion resistance and their catalytic properties, alloys based on the Mo-Pt system are used in many applications such as the glass industry, superconductivity and as catalysts [1-3]. Recently the application of the inter-metallic phases of this system as cathode material in the process of electrocatalytic hydrogen production has been reported [4-6].

The generally accepted assessed phase diagram for the Mo–Pt system shown in Fig. 1 was proposed by Brewer et al. [7]. The different phases are listed in Table 1. In addition to the terminal solid solutions bcc Mo (*A*2) and fcc Pt (*A*1), the system presents a disordered hcp Mg-type phase ε (*A*3) and four intermetallic compounds, Mo_6Pt (*A*15), MoPt ($D0_{19}$), ε' (*B*19) and $MoPt_2$. The $D0_{19}$ and *B*19 phases are ordered forms of the hcp lattice and $MoPt_2$ of the fcc one. Thus the system presents three order-disorder transitions: $D0_{19}$/*A*3, *B*19/*A*3 and $MoPt_2$/*A*1.

More recently, in order to validate and complete the phase diagram proposed in Ref. [7], Benlaharche [8] carried out an experimental study using X-ray diffraction (XRD) and Electron Probe Micro Analysis (EPMA) from equilibrated alloys which provides new crystallographic and phase equilibria data on the system.

The integration of FP calculation methods for describing the thermodynamics of phases into the CALPHAD approach is very useful for assessments as it allows the estimation of metastable thermodynamics properties. In this way, the formation energies of all end-member compounds were calculated in the present work for *A*15, *B*19, $D0_{19}$ and $MoPt_2$ phases. The electronic structure and total energy calculations were based on Density Functional Theory (DFT).

The aim of the present work is to provide, for the first time, a CALPHAD modeling of the Mo-Pt system taking into account the new experimental data provided in Ref. [8] and using the results of the DFT calculations obtained in the present study.

In recent papers [9,10], the New Approach of the Compound Energy Formalism (NACEF) has been proposed and it was shown that it can be a powerful way to improve the ability of CEF to model simple or complex phases. This new approach was also used in the current modeling to model all ordered phases of the Mo-Pt system. The present work constitutes an example of the ability of NACEF to describe ordered phases with the two-sublattice (2SL) model including the order/disorder transitions.

2. Literature review

2.1 Phase equilibria data

The first phase diagram of the Mo-Pt system was compiled by Elliot [11] based on the work of Refs. [12-17]. In this first version, the system presents in addition to the terminal solid solutions an intermediate solid solution of hcp structure and one compound identified as an fcc superstructure. Later, other stable phases (*A*15, *B*19, $D0_{19}$ and $MoPt_2$) were identified by Refs. [18-21]. These results were confirmed by Ocken et al. [22] by X-ray diffraction, metallography and thermal analyses. They proposed a complete phase diagram for the first time. Using experimental techniques similar to Ref. [22] but also resistivity and hardness measurements, Flükiger et al. [23] presented a new version of the phase diagram of the Mo-Pt system up to 55 at.% Pt. From the synthesis of the works in Refs. [22,23], Brewer et al. [7] established a complete phase diagram (Fig. 1) which constitutes the currently accepted version.

More recently, in order to validate and complete the phase diagram proposed in Ref. [7], Benlaharche [8] carried out an experimental study via XRD and EPMA analysis of samples equilibrated from different heat-treatments which provides new crystallographic and phase equilibria data on the system. The main information obtained in Ref. [8] concerns the phase diagram data summarized in Table 2 and the site fractions determined by Rietveld refinement of the X-ray powder diffraction data given in Table 3. It should be noted that the results obtained in Ref. [8] indicate that the compound *B*19 disappears by a congruent reaction with DO_{19} rather than by a peritectoid reaction as mentioned in Ref. [7].

2.2 Thermodynamic data

The only experimental measurement for the enthalpy of formation of phase of the Mo-Pt system has been conducted by Benarchid et al. [24]. Using high temperature Direct Reaction Calorimetry (DRC), these authors have determined the enthalpy of formation of *A*15, $D0_{19}$, *B*19, $MoPt_2$, and *A*1 phases. Corresponding results are shown Table 4.
From FP calculations, formation enthalpies were also obtained in Refs. [25-27] for the $MoPt_2$ and *B*19 phases as indicated in Table 5.

3. First-principle calculations

It has become common practice to use data from DFT calculations to evaluate the Gibbs energy in CALPHAD description in order to complement the experimental information [28] and to provide data in the metastable composition range.

In the present work, the first principles method has been used to express the 0 K heat of formation of every full ordered configuration generated by the sublattice description of the considered phases (here: *A*15, *B*19, $D0_{19}$ and $MoPt_2$).

Present calculations are based on the density functional theory (DFT), were carried out using the VASP package [29,30]. The Generalized Gradient Approximation (GGA) was used with the Perdew-Burke-Ernzerhof (PBE) exchange and correlation energy functional [31,32]. An energy cutoff of 600 eV was used for the plane wave basis set within a high density mesh of $2\pi \cdot 0.05/Å$ units for each direction of the irreducible Brillouin generated by the Monkhorst-Pack procedure [33]. The conditions for the calculation (relaxation method, convergence accuracy) have been detailed previously [34]. All the calculations have been handled using the ZenGen code [35], for the generation of input files, the job monitoring and results analysis.

The total energies for the *A*15, *B*19, $D0_{19}$ and $MoPt_2$ phases were calculated and used to express the corresponding enthalpies of formation referred to bcc Mo and fcc Pt, as reported in Table 5 and plotted in Fig. 2.

4. Thermodynamic models

Note that to simplify the notation, the two components Mo and Pt are referred to as A and B respectively.

4.1 Solution phases

The Gibbs energy for the solution phases φ, liquid, fcc-A1, bcc-A2 and hcp-A3 are described by the substitutional solution model with Redlich–Kister polynomials for the excess Gibbs energy contribution:

$$G^{\varphi} = \sum_i x_i \, {}^0G_i^{\varphi} + RT \sum_i x_i \, \ln x_i + {}^{\mathrm{Ex}}G \tag{1}$$

$${}^{\mathrm{Ex}}G = x_{\mathrm{A}} x_{\mathrm{B}} \sum_{\upsilon=0} {}^{\nu}L^{\varphi} \left(x_{\mathrm{A}} - x_{\mathrm{B}} \right)^{\upsilon} \tag{2}$$

where x_i represents the mole fraction of the elements *i* and ${}^0G_i^{\varphi}$ is the Gibbs energy of the pure elements *i* in the structure of phase φ. ${}^{\nu}L^{\varphi}$, are the Redlich-Kister parameters representing the interaction of order ν between the two components in the φ phase and are linear functions of temperature with adjustable parameters.

4.2 *A*15, *D*0$_{19}$, *B*19 and MoPt$_2$ phases

The four ordered phases are modeled by the 2SL model $(\mathrm{A,B})_a(\mathrm{A,B})_b$ with the multiplicity $a = 3b$ for *A*15 and *D*0$_{19}$, $a = 2b$ for MoPt$_2$ and $a = b$ for *B*19 using the NACEF approach [9].

In CEF or NACEF approach, the corresponding Gibbs energy is given by:

$$G^{\varphi} = {}^{\mathrm{Cfg}}G + {}^{\mathrm{Ref}}G + {}^{\mathrm{Ex}}G \tag{3}$$

$${}^{\mathrm{Cfg}}G = \frac{RT}{a+b}\left(a\sum_i y_i^{(1)} \ln y_i^{(1)} + b\sum_i y_i^{(2)} \ln y_i^{(2)} \right) \tag{4}$$

$${}^{\mathrm{Ref}}G = \sum_i x_i \, {}^0G_i^{\varphi} \tag{5}$$

where ${}^0G_i^{\varphi}$ is the Gibbs energy of the pure elements *i* in the structure of phase φ and y_i^s the mole fraction of element *i* in sublattice *s*.

In the CEF, the excess contribution is described by:

$$\begin{aligned} {}^{\mathrm{Ex}}G = & \sum_{i,j} y_i^{(1)} y_j^{(2)} \Delta G_{i:j} \\ & + y_{\mathrm{A}}^{(1)} y_{\mathrm{B}}^{(1)} \sum_i y_i^{(2)} \sum_{\upsilon=0} {}^{\upsilon}L_{\mathrm{A,B}:i} \left(y_{\mathrm{A}}^{(1)} - y_{\mathrm{B}}^{(1)} \right)^{\upsilon} + \ldots \\ & + y_{\mathrm{A}}^{(1)} y_{\mathrm{B}}^{(1)} y_{\mathrm{A}}^{(2)} y_{\mathrm{B}}^{(2)} L_{\mathrm{A,B:A,B}} \end{aligned} \tag{6}$$

where $\Delta G_{i:j}$ is the Gibbs energy of formation of the $i_a \, j_b$ compound referred to the reference states of the elements, ${}^{\upsilon}L_{\mathrm{A,B}:i}$ and $L_{\mathrm{A,B:A,B}}$ are interaction parameters.

For phases with order/disorder transitions the partitioning [36] of the Gibbs-energy expression is into two parts as follows:

$${}^{\mathrm{Ex}}G = G^{\mathrm{dis}}(x_i) + \Delta G^{\mathrm{ord}}(y_i^s) \tag{7}$$

$$\Delta G^{\mathrm{ord}}(y_i^s) = G^{\mathrm{ord}}(y_i^s) - G^{\mathrm{ord}}(y_i^s = x_i) \tag{8}$$

where $G^{\mathrm{dis}}(x_i)$ is the excess Gibbs energy of the disordered state and it is expressed by a Redlich-Kister polynomial (Eq. 2). $\Delta G^{\mathrm{ord}}(y_i^s)$ is the part giving the excess contribution due to

long-range ordering depending on the four site fractions y_i^s. Thus, the parameters of both ordered and disordered phases can be evaluated independently.

In the NACEF approach, disordered and ordered contributions which are intrinsically contained in the excess term given by Eq. (6) are separated without the use of the partitioning (Eqs. 7-8) as follows:

$$^{\mathrm{Ex}}G = G^{\mathrm{dis}}(x_i) + G^{\mathrm{ord}}(\eta) \tag{9}$$

with

$$G^{\mathrm{dis}}(x_i) = x_{\mathrm{A}}x_{\mathrm{B}}\left[P0 + P1\left(x_{\mathrm{A}} - x_{\mathrm{B}}\right) + P2\left(x_{\mathrm{A}} - x_{\mathrm{B}}\right)^2\right] \tag{10}$$

$$\begin{aligned} G^{\mathrm{ord}}(\eta) = \eta & \left[P10 + P11\left(x_{\mathrm{A}} - x_{\mathrm{B}}\right) + P12\left(x_{\mathrm{A}} - x_{\mathrm{B}}\right)^2 + P13\left(x_{\mathrm{A}} - x_{\mathrm{B}}\right)^3\right] \\ & + \eta^2\left[P20 + P21\left(x_{\mathrm{A}} - x_{\mathrm{B}}\right) + P22\left(x_{\mathrm{A}} - x_{\mathrm{B}}\right)^2\right] \\ & + \eta^3\left[P30 + P31\left(x_{\mathrm{A}} - x_{\mathrm{B}}\right)\right] \\ & + \eta^4\left[P40\right] \end{aligned} \tag{11}$$

where η is the Bragg–Williams Long Range Order (LRO) parameter which describes the ordering and which can be expressed as follows [9]:

$$\eta = \frac{(a+b)}{b}\left(y_{\mathrm{B}}^{(1)} - x_{\mathrm{B}}\right) \tag{12}$$

The phase is disordered when $\eta = 0$ and when $a \geq b$, the totally ordered configurations $\mathrm{B}_a\mathrm{A}_b$ and $\mathrm{A}_a\mathrm{B}_b$ are obtained when $\eta = 1$ and $\eta = -1$ respectively.

All the NACEF parameters, $P\nu$ for the disordered part and $P\lambda\mu$ for the ordered one, are obtained from the CEF parameters via the $\left[\mathrm{Q}_{a:b}\right]$ matrix defined as follows:

$$\begin{bmatrix} P10 \\ P11 \\ P12 \\ P13 \\ P20 \\ P21 \\ P22 \\ P30 \\ P31 \\ P40 \\ P0 \\ P1 \\ P2 \end{bmatrix} = \left[\mathrm{Q}_{a:b}\right] \times \begin{bmatrix} \Delta G_{\mathrm{A:B}} \\ \Delta G_{\mathrm{B:A}} \\ {}^0L_{\mathrm{A,B:A}} \\ {}^0L_{\mathrm{A,B:B}} \\ {}^0L_{\mathrm{A:A,B}} \\ {}^0L_{\mathrm{B:A,B}} \\ {}^1L_{\mathrm{A,B:A}} \\ {}^1L_{\mathrm{A,B:B}} \\ {}^1L_{\mathrm{A:A,B}} \\ {}^1L_{\mathrm{B:A,B}} \\ {}^2L_{\mathrm{A,B:*}} \\ {}^2L_{\mathrm{*:A,B}} \\ L_{\mathrm{A,B:A,B}} \end{bmatrix} \tag{13}$$

In the NACEF approach, the corresponding parameters are optimized directly and independently. This is made possible by the fact that the matrix $\left[\mathrm{Q}_{a:b}\right]$ which is square can be

inverted because, whatever the site multiplicities *a* and *b*, its determinant is nonzero. This leads to express the CEF parameters using the matrix $\left[\mathrm{P}_{a:b}\right]=\left[\mathrm{Q}_{a:b}\right]^{-1}$ defined as follows:

$$\begin{bmatrix} \Delta G_{\mathrm{A:B}} \\ \Delta G_{\mathrm{B:A}} \\ {}^{0}L_{\mathrm{A,B:A}} \\ {}^{0}L_{\mathrm{A,B:B}} \\ {}^{0}L_{\mathrm{A:A,B}} \\ {}^{0}L_{\mathrm{B:A,B}} \\ {}^{1}L_{\mathrm{A,B:A}} \\ {}^{1}L_{\mathrm{A,B:B}} \\ {}^{1}L_{\mathrm{A:A,B}} \\ {}^{1}L_{\mathrm{B:A,B}} \\ {}^{2}L_{\mathrm{A,B:*}} \\ {}^{2}L_{\mathrm{*:A,B}} \\ L_{\mathrm{A,B:A,B}} \end{bmatrix} = \left[\mathrm{P}_{a:b}\right] \times \begin{bmatrix} P10 \\ P11 \\ P12 \\ P13 \\ P20 \\ P21 \\ P22 \\ P30 \\ P31 \\ P40 \\ P0 \\ P1 \\ P2 \end{bmatrix} \tag{14}$$

The previous equation allows the use of the NACEF approach in a database usable by a thermodynamic calculation software using the CEF model. Furthermore, they give the relationships which express the Gibbs energies of the compounds from the NACEF parameters: $\Delta G_{i:j} = f\left(P\lambda\mu, P\nu\right)$

The matrix $\left[\mathrm{P}_{a:b}\right]$ thus obtained for the *A*15, $D0_{19}$, *B*19 and $MoPt_2$ phases are given in Appendix A according to the corresponding site multiplicities *a* and *b*.

Moreover, it was shown in Ref. [9] that in the case of an order-disorder transition, all the $P\lambda\mu$ parameters with $\lambda = 1$ must be zero: $P10 = P11 = P12 = P13 = 0$.

In the case of the *B*19 phase, the symmetry of the two crystallographic sites implies that the $P\lambda\mu$ parameters with $\lambda = 3$ must be zero: $P30 = P31 = 0$.

Finally, the Gibbs energies of the compounds for the four ordered phases are reduced to the expressions given in Table 6.

5. Results

The PARROT module of Thermo-Calc [37] was employed to evaluate the model parameters in Gibbs energy function from the thermochemical, structural and phase equilibria data. The Gibbs energy descriptions for hcp, fcc, bcc and liquid phases of pure Mo and pure Pt are taken from the SGTE PURE element database [38]. The values of all assessed thermodynamic parameters for the Mo–Pt system obtained in the present work are listed in Table 7. The complete thermodynamic database is provided in Thermo-Calc format in Appendix B and as supplementary materials.

The description of the $MoPt_2$ phase which is a superstructure of fcc requires that its disordered part corresponds to the *A*1 phase. Thus, in the modeling of the order/disorder transition $MoPt_2$/*A*1 from CEF or NACEF, phases *A*1 and $MoPt_2$ correspond to two distinct

compositions of the same Gibbs function. This can be a problem if other fcc superstructures have to be taken into account in a multi-component database. In the present work, in order to consider these two phases separately, phase *A*1 is described from another function whose Gibbs energy of mixing is identical to the disordered part of $MoPt_2$. However, in order to distinguish this *A*1 phase from the disordered part of $MoPt_2$ in the equilibrium calculations, the energies of the pure elements in the $MoPt_2$ structure are made less stable by 0.01 J/mol than those in the *A*1 structure (see Table 7). The same treatment was applied to *A*3 phase in the case of transitions $D0_{19}$/*A*3 and *B*19/*A*3 for which $D0_{19}$ and *B*19 have the same energies in the disordered states.
The phase diagram for the Mo–Pt system from the present CALPHAD modeling is shown in Fig. 3 and in Fig. 4 with the superimposed experimental data. Temperatures of invariant equilibria calculated in the current assessment are compared to those proposed in Ref. [7] in Table 8. It should be noted that the phase diagram data in Ref. [8] are consistent with those of Ref. [7] except for the *B*19 phase. Indeed, according to Ref. [7], *B*19 decomposes upon heating by a peritectoid reaction while the data from Ref. [8] shows that it decomposes in a congruent manner, which was considered in the present evaluation. So, one can observe that the calculation reproduces the experimental data of phase boundaries and the temperatures of invariant equilibria relatively well if we consider the uncertainties of such kind data.
The FP enthalpies of formation and the corresponding values calculated thanks to relationships given in Table 6 are compared in Table 5 and are plotted in Fig. 5 along with the enthalpies of formation calculated at 1 K for all solid phases of the system. We can thus observe for all the compounds (end-members) the very good restitution of the DFT data by the present modeling based on the NACEF approach in which these values are considered as input data and not as parameters.
Enthalpies of formation based on high temperature DRC measurements provided in Ref. [24] are compared with those calculated from the current modeling in Table 4. It should be noted that although the agreement is relatively satisfactory, these data were considered during the optimization with a low weight compared to the DFT data.
The calculated site occupancies of the $D0_{19}$, *B*19 and $MoPt_2$ phases are given Fig. 6 along with the corresponding experimental data from Ref. [8]. We can thus also observe the very good agreement of these structural data by the present modeling.

6. Conclusion

In the present work, a thermodynamic description of the Mo–Pt system, which exhibits three order/disorder transformation, is obtained using a combined FP/CALPHAD approach. The liquid, fcc, bcc and hcp phases were treated with a substitution solution model and *A*15, *B*19, $D0_{19}$ and $MoPt_2$ compounds were described with a 2SL model within the framework of the NACEF approach. FP calculations were performed to obtain the enthalpies of formation for all the end-member compounds of the *A*15, *B*19, $D0_{19}$ and $MoPt_2$ phases at 0 K and were used with phase equilibria and site occupancy experimental data to evaluate the model parameters. The calculated results obtained from the present description of the Mo-Pt system show a very good agreement with all the various data and this is obtained with a limited number of assessed parameters. The result thus obtained highlights the ability of NACEF to take into account order/disorder transformations in a simple and effective manner.

Declaration of competing interest

The authors declare no conflict of interest.

Acknowledgments

DFT calculations were performed using HPC resources from GENCI-CINES (Grant 2019-096175).

The authors acknowledge the French consortium in Thermodynamics of Materials AFTherMat (https://www.afthermat.fr/), where constructive exchanges led to the present collaborative work.

Appendix A

Matrix

Appendix B

Thermodynamic database (TDB files):

Supplementary material

Thermodynamic database (TDB files):

References

[1] G.L. Selman, Platinum Metals Rev., 11 (4) (1967) 132-137.
[2] B.N. Grgur, G. Zhuang, N.M. Markovic, P.N. Ross, J. Phys. Chem. B, 101 (20) (1997) 3910–3913.
[3] R. Flukiger, A. Paoli, R. Roggen, K. Yvon, J. Muller, Solid State Commun., 11 (1) (1972) 61–63.
[4] M. P. Marčeta Kaninski, D. L. Stojić, D. P. Saponjić, N. I. Potkonjak, and S. S. Miljanić, J. Power Sources, 157 (2) (2006) 758-764.
[5] D. Stojic, T. D. Grozdic, M. P. Marceta Kaninski, A. D. Maksic, N. D. Simic, International J. Hydrogen Energy, 31 (7) (2006) 841-846.
[6] D. Stojic, T. D. Grozdic, M. P. Marceta Kaninski, V. D. Stanic, International J. Hydrogen Energy, 32 (13) (2007) 2314-2319.
[7] L. Brewer, R.H. Lamoreaux, Bull. Alloy Phase Diagrams, 1 (1980) 89-91.
[8] T. Benlaharche, Etude et modélisation thermodynamique du système Mo-Pt-Si, [PHD] Nancy I University (France), (2008).
[9] J. M. Fiorani, M. Badran, A. A. A. P. Da Silva, N. David, and M. Vilasi, CALPHAD, 80 (2023) 102509.
[10] J.M. Fiorani, M. Badran, J.M. Joubert, J.C. Crivello, A.A.A.P da Silva, G.C. Coelho, C.A. Nunes, N. David, M. Vilasi, CALPHAD, 80 (2023) 102522.
[11] R.P. Elliott et al., Constitution of Binary Alloys, First Supplement (1965).
[12] E. Raub, Z. Metallk., 45 (1954) 23.
[13] H. Nishimura, Nippon Kinzoku Gakkaishi, 22 (1958) 525-428.
[14] H. Nishimura, H. Kimura, Nippon Kinzoku Gakkaishi, 23 (1959) 616-620.
[15] A. G. Knapton, J. Ind. Metals, 87 (1959) 28-32.
[16] A. G. Knapton, Planseeber. Pulvermet., 7 (1959) 2-3.
[17] H. Kimura, Trans. Natl. Res. Ind. Metals, 2 (1) (1960) 30-36.
[18] H. G. Meissner, M. Potzsche, W. Rossteutscher, E. Stolz, Naturwissenschaften, 49 (1962) 57.
[19] H.P. Rooksby, B. Lewis, J. Less-Common Met., 6 (1964) 451.
[20] A. Maldano, K. Schubert, Z. Metallk., 55 (1964) 619.
[21] G. L. Selman, Platinum Metals Rev., 11 (1967) 132.
[22] H. Ocken, J.H.N. Van Vucht, J. Less-Common Met., 15 (1968) 193.
[23] R. Flükiger, K. Yvon, C. Susz, R. Roggen, A. Paoli, J. Muller, J. Less-Common Met., 32 (1973) 207.
[24] My. Y. Benarchid, N. David, J.-M. Fiorani, M. Vilasi, and T. Benlaharche, The J. of Chemical Thermodynamics, 41 (3) (2009) 383-385.
[25] M. Stojkovic´, V. Koteski, J. Beloševic´ -Cˇavor, B. Cekic´, D. Stojic´, V. Ivanovski, Phys. Rev. B, 77 (2008) 193111/1-193111/4.
[26] S. Curtarolo, D. Morgan, G. Ceder, CALPHAD 29 (2005) 163-211.
[27] Z.W. Lu, B.M. Klein, Phys. Rev. B, 50 (1994) 5962-5970.
[28] Z.-K. Liu, J. Phase Equilibria Diffusion, 30 (2009) 517.
[29] G. Kresse and J. Furthmüller, Phys. Rev. B, 54 (1996) 11169.
[30] G. Kresse and D. Joubert, Phys. Rev. B, 59 (1999) 1758.
[31] J. P. Perdew, K. Burke, and M. Ernzerhof. Phys. Rev. Lett., 77 (1996) 3865.
[32] J. P. Perdew, K. Burke, and M. Ernzerhof. Phys. Rev. Lett., 78 (1997) 1396.
[33] Monkhorst, H. & Pack, Phys. Rev. B, 13 (1976) 5188-5192.
[34] J.C. Crivello, M. Palumbo, T. Abe, J.M. Joubert, CALPHAD, 34 (2010) 487-494.
[35] J.C. Crivello, R. Souques, A. Breidi, N. Bourgeois, J.M. Joubert, CALPHAD, 51 (2015) 233-240.
[36] I. Ansara, N. Dupin, H.L. Lukas, B. Sundman, J. of Alloys and Compounds, 247 (1-2) (1997) 20-30.
[37] B. Sundman, B. Jansson, J.O. Andersson, CALPHAD, 9 (2) (1985) 153-190.
[38] A.T. Dinsdale, CALPHAD, 15 (4) (1991) 317-425.

Appendix A

$[P_{a:b}]$ matrix resulting from the NACEF approach for the 2SL model $(A,B)_a(A,B)_b$.

$$[P_{3:1}] = \begin{bmatrix}
-1 & -1/2 & -1/4 & -1/8 & 1 & 1/2 & 1/4 & -1 & -1/2 & 1 & 3/16 & 3/32 & 3/64 \\
1 & -1/2 & 1/4 & -1/8 & 1 & -1/2 & 1/4 & 1 & -1/2 & 1 & 3/16 & -3/32 & 3/64 \\
0 & 3/2 & -3/8 & 9/32 & -1 & 5/4 & -7/16 & -3/2 & 9/8 & -7/4 & 9/16 & 27/64 & -9/256 \\
0 & 3/2 & 3/8 & 9/32 & -1 & -5/4 & -7/16 & 3/2 & 9/8 & -7/4 & 9/16 & -27/64 & -9/256 \\
0 & -1/2 & -5/8 & -19/32 & -1 & -1/4 & 1/16 & 3/2 & 5/8 & -7/4 & 1/16 & 9/64 & 39/256 \\
0 & -1/2 & 5/8 & -19/32 & -1 & 1/4 & 1/16 & -3/2 & 5/8 & -7/4 & 1/16 & -9/64 & 39/256 \\
0 & 0 & 9/8 & 0 & 0 & -3/4 & 3/4 & 1/2 & -1 & 1 & 0 & 27/64 & 27/64 \\
0 & 0 & 9/8 & 0 & 0 & -3/4 & -3/4 & 1/2 & 1 & -1 & 0 & 27/64 & -27/64 \\
0 & 0 & -1/8 & -1/4 & 0 & -1/4 & -1/4 & -1/2 & 0 & 1 & 0 & 1/64 & 3/64 \\
0 & 0 & -1/8 & 1/4 & 0 & -1/4 & 1/4 & -1/2 & 0 & -1 & 0 & 1/64 & -3/64 \\
0 & 0 & 0 & 27/32 & 0 & 0 & -9/16 & 0 & 3/8 & -1/4 & 0 & 0 & 81/256 \\
0 & 0 & 0 & -1/32 & 0 & 0 & -1/16 & 0 & -1/8 & -1/4 & 0 & 0 & 1/256 \\
0 & 0 & 0 & 9/4 & 0 & 0 & -1/2 & 0 & -3 & 6 & 0 & 0 & -27/32
\end{bmatrix}$$

$$[P_{2:1}] = \begin{bmatrix}
-1 & -1/3 & -1/9 & -1/27 & 1 & 1/3 & 1/9 & -1 & -1/3 & 1 & 2/9 & 2/27 & 2/81 \\
1 & -1/3 & 1/9 & -1/27 & 1 & -1/3 & 1/9 & 1 & -1/3 & 1 & 2/9 & -2/27 & 2/81 \\
0 & 4/3 & 0 & 4/27 & -1 & 1 & -1/9 & -3/2 & 5/6 & -7/4 & 4/9 & 4/9 & 4/81 \\
0 & 4/3 & 0 & 4/27 & -1 & -1 & -1/9 & 3/2 & 5/6 & -7/4 & 4/9 & -4/9 & 4/81 \\
0 & -2/3 & -2/3 & -14/27 & -1 & 0 & 2/9 & 3/2 & 1/3 & -7/4 & 1/9 & 2/9 & 16/81 \\
0 & -2/3 & 2/3 & -14/27 & -1 & 0 & 2/9 & -3/2 & 1/3 & -7/4 & 1/9 & -2/9 & 16/81 \\
0 & 0 & 8/9 & 8/27 & 0 & -2/3 & 4/9 & 1/2 & -5/6 & 1 & 0 & 8/27 & 32/81 \\
0 & 0 & 8/9 & -8/27 & 0 & -2/3 & -4/9 & 1/2 & 5/6 & -1 & 0 & 8/27 & -32/81 \\
0 & 0 & -2/9 & -10/27 & 0 & -1/3 & -2/9 & -1/2 & 1/6 & 1 & 0 & 1/27 & 8/81 \\
0 & 0 & -2/9 & 10/27 & 0 & -1/3 & 2/9 & -1/2 & -1/6 & -1 & 0 & 1/27 & -8/81 \\
0 & 0 & 0 & 16/27 & 0 & 0 & -4/9 & 0 & 1/3 & -1/4 & 0 & 0 & 16/81 \\
0 & 0 & 0 & -2/27 & 0 & 0 & -1/9 & 0 & -1/6 & -1/4 & 0 & 0 & 1/81 \\
0 & 0 & 0 & 16/9 & 0 & 0 & -4/3 & 0 & -2 & 6 & 0 & 0 & -32/27
\end{bmatrix}$$

$$[P_{1:1}] = \begin{bmatrix} -1 & 0 & 0 & 0 & 1 & 0 & 0 & -1 & 0 & 1 & 1/4 & 0 & 0 \\ 1 & 0 & 0 & 0 & 1 & 0 & 0 & 1 & 0 & 1 & 1/4 & 0 & 0 \\ 0 & 1 & 1/2 & 1/4 & -1 & 1/2 & 1/4 & -3/2 & 1/4 & -7/4 & 1/4 & 3/8 & 3/16 \\ 0 & 1 & -1/2 & 1/4 & -1 & -1/2 & 1/4 & 3/2 & 1/4 & -7/4 & 1/4 & -3/8 & 3/16 \\ 0 & -1 & -1/2 & -1/4 & -1 & 1/2 & 1/4 & 3/2 & -1/4 & -7/4 & 1/4 & 3/8 & 3/16 \\ 0 & -1 & 1/2 & -1/4 & -1 & -1/2 & 1/4 & -3/2 & -1/4 & -7/4 & 1/4 & -3/8 & 3/16 \\ 0 & 0 & 1/2 & 1/2 & 0 & -1/2 & 0 & 1/2 & -1/2 & 1 & 0 & 1/8 & 1/4 \\ 0 & 0 & 1/2 & -1/2 & 0 & -1/2 & 0 & 1/2 & 1/2 & -1 & 0 & 1/8 & -1/4 \\ 0 & 0 & -1/2 & -1/2 & 0 & -1/2 & 0 & -1/2 & 1/2 & 1 & 0 & 1/8 & 1/4 \\ 0 & 0 & -1/2 & 1/2 & 0 & -1/2 & 0 & -1/2 & -1/2 & -1 & 0 & 1/8 & -1/4 \\ 0 & 0 & 0 & 1/4 & 0 & 0 & -1/4 & 0 & 1/4 & -1/4 & 0 & 0 & 1/16 \\ 0 & 0 & 0 & -1/4 & 0 & 0 & -1/4 & 0 & -1/4 & -1/4 & 0 & 0 & 1/16 \\ 0 & 0 & 0 & 0 & 0 & 0 & -2 & 0 & 0 & 6 & 0 & 0 & -3/2 \end{bmatrix}$$

Table 1

Crystallographic informations of stable solid phases of the Mo-Pt system.
(SD=Strukturbericht Designation; PS= Pearson Symbol; SG=Space Group; P=Prototype; WP=Wyckoff position)

Phase	PS	SG	P	SD	WP
(Mo)	*cI*2	*Im*-3*m*	W	*A*2	2*a*
Mo_6Pt	*cP*8	*Pm*-3*n*	Cr_3Si	*A*15	6*c* : 2*a*
ε	*hP*2	*P*6$_3$/*mmc*	Mg	*A*3	2*c*
ε’	*hP*8	*P*6$_3$/*mmc*	Ni_3Sn	$D0_{19}$	6*h* : 2*c*
MoPt	*oP*4	*Pmma*	AuCd	*B*19	2*e* : 2*f*
$MoPt_2$	*oI*6	*Immm*	$MoPt_2$		2*a* : 4*g*
(Pt)	*cF*4	*Fm*-3*m*	Cu	*A*1	2*a*

Table 2
Diagram data from Ref. [8].

T (K)	N°	Phases	% at. Pt	T (K)	N°	Phases	% at. Pt
1473	1	*D*0$_{19}$	39.8	1623	17	*A*2	2.9
	2	*B*19	44.4			*A*15	18.5
	3		47.4		18	*A*15	19.0
	4	*B*19 MoPt$_2$	48.9			*D*0$_{19}$	35.6
			62.2		19	*D*0$_{19}$	36.7
	5		48.5		20		41.4
			61.9		21		43.3
	6		49.0		22		47.0
			61.8		23		49.2
	7	MoPt$_2$	63.1		24	*D*0$_{19}$	51.3
	8		67.3			MoPt$_2$	61.6
1548	9	*A*2	2.8		25	MoPt$_2$	63.9
		*D*0$_{19}$	36.6		26		68.6
	10	*D*0$_{19}$	43.3		27	MoPt$_2$	69.1
	11		43.6			*A*1	74.4
	12	*B*19	48.3	1953	28	*A*2	8.1
	13	*D*0$_{19}$ MoPt$_2$	51.1			*A*15	18.5
			61.8		29	*A*15	18.3
	14		51.0			*D*0$_{19}$	33.5
			61.8		30	MoPt$_2$	64.2
	15	MoPt$_2$	64.3				
	16		68.3				

Table 3
Site occupancies from Ref. [8].

Phase	T (K)	at. % Pt	Site fractions			
			Mo-4*g*	Pt-4*g*	Mo-2*a*	Pt-2*a*
$MoPt_2$	1623	63.87	0.065	0.935	0.9535	0.0465
	1623	68.57	0.0625	0.9375	0.82	0.18
	1953	64.2	0.095	0.905	0.885	0.115
			Mo-2*e*	Pt-2*e*	Mo-2*f*	Pt-2*f*
*B*19	1473	44.43	0.97	0.03	0.14	0.86
	1473	47.36	0.96	0.04	0.093	0.907
			Mo-6*h*	Pt-6*h*	Mo-2*c*	Pt-2*c*
$D0_{19}$	1623	43.34	0.75	0.25	0.015	0.985

Table 4
Enthalpy of formation (kJ/mol) ΔH based on high temperature direct reaction calorimetry data obtained by [24] and calculated from the Present Modeling [PM]. Reference states are bcc Mo and fcc Pt at the considered temperature.

Phase		*A*15	$D0_{19}$	*B*19	$MoPt_2$	*A*1
X(Pt)		0.1913	0.3663	0.4522	0.6364	0.7304
T (K)		1768	298.15	298.15	298.15	298.15
ΔH	[24]	-13.0±1.9	-26.1±4.9	-27.7±3.9	-36.9±1.8	-27.1±4.2
	[PM]	-7.4	-17.9	-26.7	-32.8	-25.6

Table 5

FP enthalpies of formation (kJ/mol) and corresponding results calculated from the present CALPHAD assessment referred to bcc Mo and fcc Pt.

Phase	X(Pt)	This work		[27]	[26]	[25]
		DFT	CALPHAD	DFT	DFT	DFT
$MoPt_2$	0.333	-4.049	-4.053			
	0.667	-34.707	-34.639	-37.6	-37.6	-37.6
$D0_{19}$	0.25	-6.445	-6.409			
	0.75	-22.005	-22.026			
$B19$	0.5	-30.661	-30.650	-34.4		
$A15$	0	8.582	8.582			
	0.25	-10.828	-10.839			
	0.75	-10.444	-10.437			
	1	24.663	24.663			

Table 6

Gibbs energies of formation $\Delta G_{i:j}$ of the compounds (end-members) of the four ordered phases expressed from the NACEF parameters.

Phase	$\Delta G_{i:j}$
$A15$ and $D0_{19}$	$\Delta G_{\mathrm{A:B}} = \frac{3}{16}\left(P0 + \frac{1}{2}P1 + \frac{1}{4}P2\right) + P20 + \frac{1}{2}P21 + \frac{1}{4}P22 - P30 - \frac{1}{2}P31 + P40$
	$\Delta G_{\mathrm{B:A}} = \frac{3}{16}\left(P0 - \frac{1}{2}P1 + \frac{1}{4}P2\right) + P20 - \frac{1}{2}P21 + \frac{1}{4}P22 + P30 - \frac{1}{2}P31 + P40$
$B19$	$\Delta G_{\mathrm{A:B}} = \Delta G_{\mathrm{B:A}} = \frac{1}{4}P0 + P20 + P40$
$MoPt_2$	$\Delta G_{\mathrm{A:B}} = \frac{2}{9}\left(P0 + \frac{1}{3}P1 + \frac{1}{9}P2\right) + P20 + \frac{1}{3}P21 + \frac{1}{9}P22 - P30 - \frac{1}{3}P31 + P40$
	$\Delta G_{\mathrm{B:A}} = \frac{2}{9}\left(P0 - \frac{1}{3}P1 + \frac{1}{9}P2\right) + P20 - \frac{1}{3}P21 + \frac{1}{9}P22 + P30 - \frac{1}{3}P31 + P40$

Table 7

Thermodynamic parameters for the phases of the Mo–Pt system obtained in the present work (J/mol atoms). The parameters for the pure elements in fcc, bcc, hcp and liquid structure where taken form the SGTE unary PURE database [38].

Solutions φ				
	Liquid	fcc-A1	bcc-A2	hcp-A3
${}^0G^{\varphi}_{\mathrm{Mo}}$	GLIQMO	GFCCMO	GHSERMO	GHCPMO
${}^0G^{\varphi}_{\mathrm{Pt}}$	GLIQPT	GHSERPT	GBCCPT	GHCPPT
${}^0L^{\varphi}$	-113238+18.321 *T*	-117910+10.135 *T*	-31710-11.522 *T*	-112163+8.097 *T*
${}^1L^{\varphi}$	19914	71042-25.3 *T*	24753	73915-26.991 *T*
${}^2L^{\varphi}$	-14515			13390

Compounds φ				
	$MoPt_2$	$D0_{19}$	*B*19	*A*15
	$(Mo,Pt)_2^{4g}(Mo,Pt)_1^{2a}$	$(Mo,Pt)_3^{6h}(Mo,Pt)_1^{2c}$	$(Mo,Pt)_1^{2e}(Mo,Pt)_1^{2f}$	$(Mo,Pt)_3^{6c}(Mo,Pt)_1^{2a}$
${}^0G^{\varphi}_{\mathrm{Mo}}$	GFCCMO+0.01	GHCPMO+0.01	GHCPMO+0.01	GHSERMO+8582
${}^0G^{\varphi}_{\mathrm{Pt}}$	GHSERPT+0.01	GHCPPT+0.01	GHCPPT+0.01	GHSERPT+24663
P0	${}^0L^{\text{fcc-A1}}$	${}^0L^{\text{hcp-A3}}$	${}^0L^{\text{hcp-A3}}$	-14990
P1	${}^1L^{\text{fcc-A1}}$	${}^1L^{\text{hcp-A3}}$	${}^1L^{\text{hcp-A3}}$	
P2	${}^2L^{\text{fcc-A1}}$	${}^2L^{\text{hcp-A3}}$	${}^2L^{\text{hcp-A3}}$	
P10				-3819
P11				29557+3.162 *T*
P20	4085	-5481+0.497 *T*	-6885-0.421 *T*	-9672-0.45 *T*
P21	14531		-10632	
P22	44601	33162-14.884 *T*	21029	
P30	-2653-10.286 *T*	1384		
P31	19364			
P40	-3330+9.954 *T*	-3649	-2749+1.221 *T*	

Table 8
Temperatures of invariant equilibria calculated in This Work [TW] compared to those proposed in Ref. [7].

Equilibrium			T (K)	
φ_1	φ_2	φ_3	[TW]	[7]
*A*3	Liq		2446	2448 ±20
*A*2	Liq	*A*3	2355	2353 ±20
*A*3	*A*1	Liq	2296	2293 ±20
*A*2	$D0_{19}$	*A*3	2154	2153 ±30
$MoPt_2$	*A*1		2073	2073 ±20
*A*2	*A*15	$D0_{19}$	2048	2053 ±20
*A*3	*A*1	$MoPt_2$	1872	1873 ±30
$D0_{19}$	*A*3	$MoPt_2$	1740	1748 ±20
*B*19	$D0_{19}$		1591	
$D0_{19}$	*B*19	$MoPt_2$		1573±20
*A*2	*A*15	$D0_{19}$	1556	1553 ±10
*B*19	$D0_{19}$	$MoPt_2$	1519	
*A*2	$D0_{19}$	*B*19	1158	

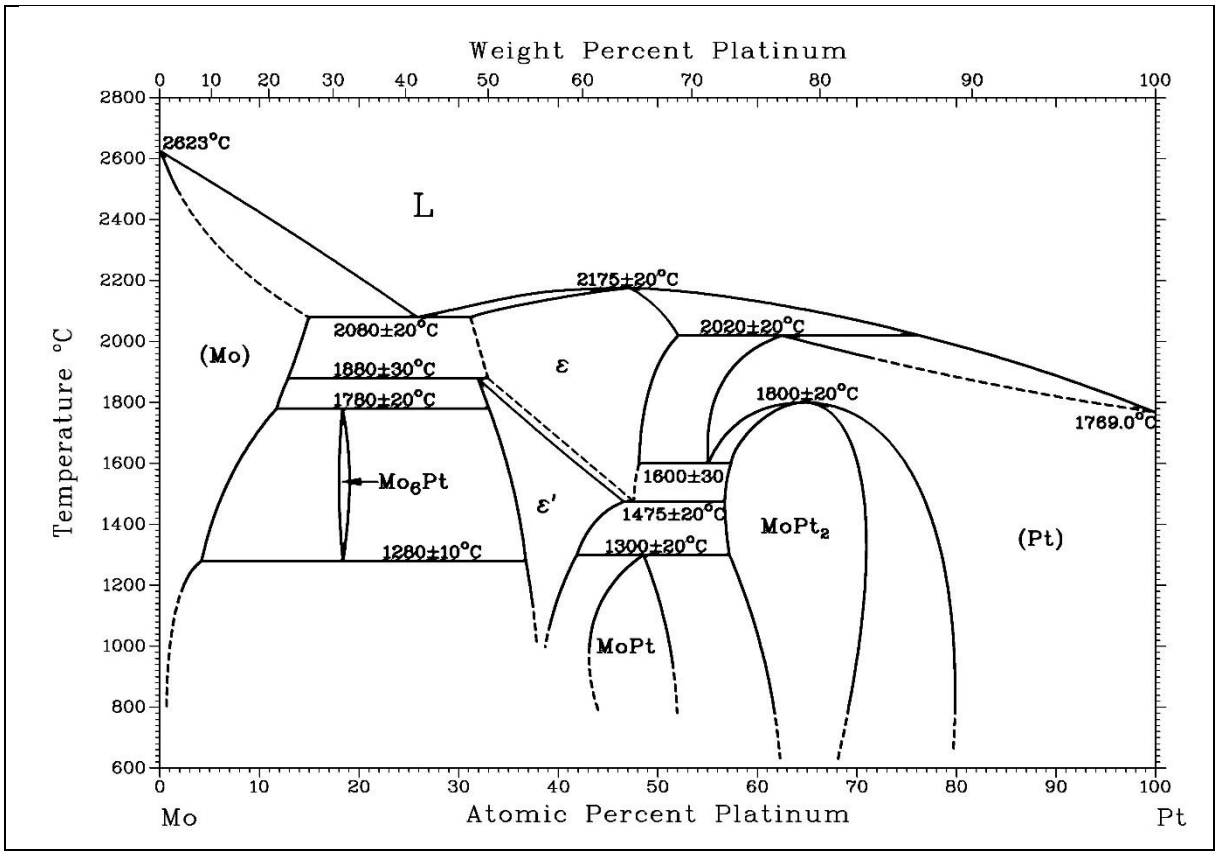

Fig. 1. The Mo–Pt phase diagram reported Ref. [7].

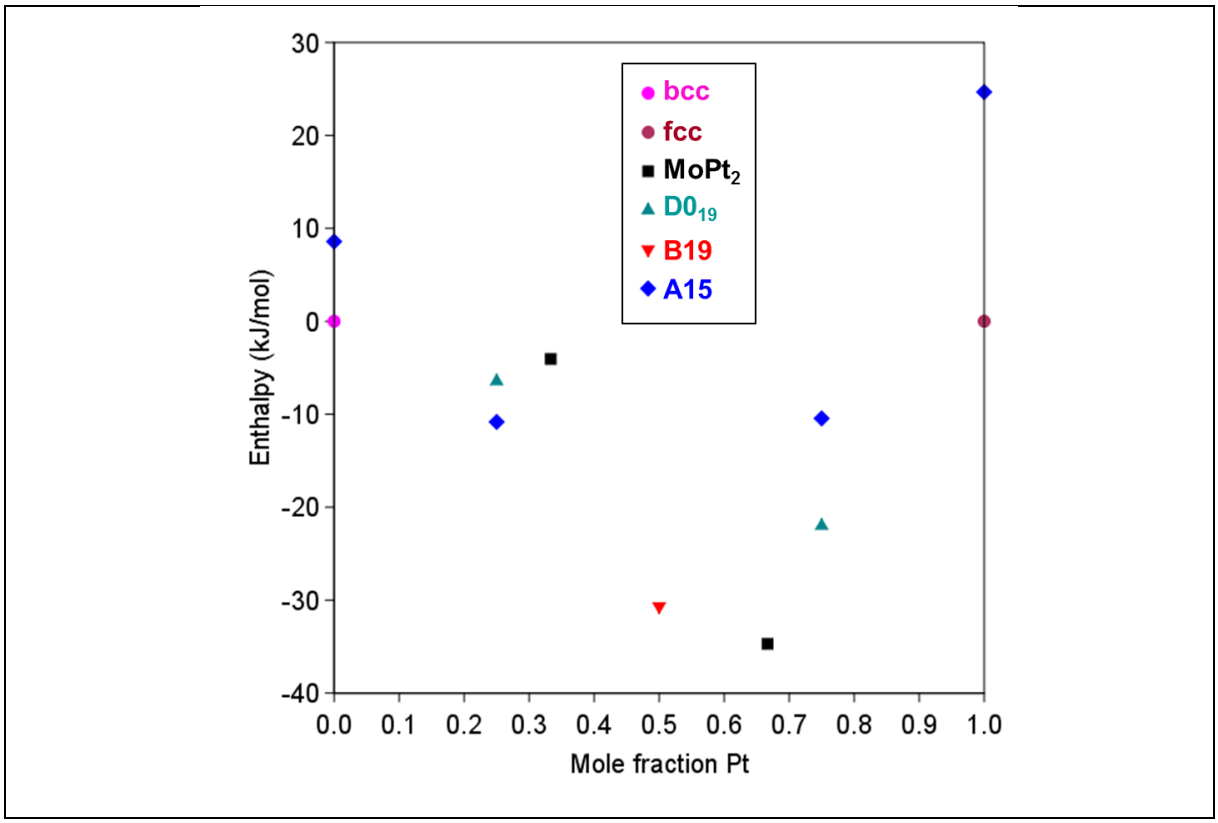

Fig. 2. FP enthalpies of formation at 0 K of the ordered configurations of the $MoPt_2$, $D0_{19}$, $B19$ and $A15$ phases obtained in the present work. The reference state is bcc for Mo and fcc for Pt.

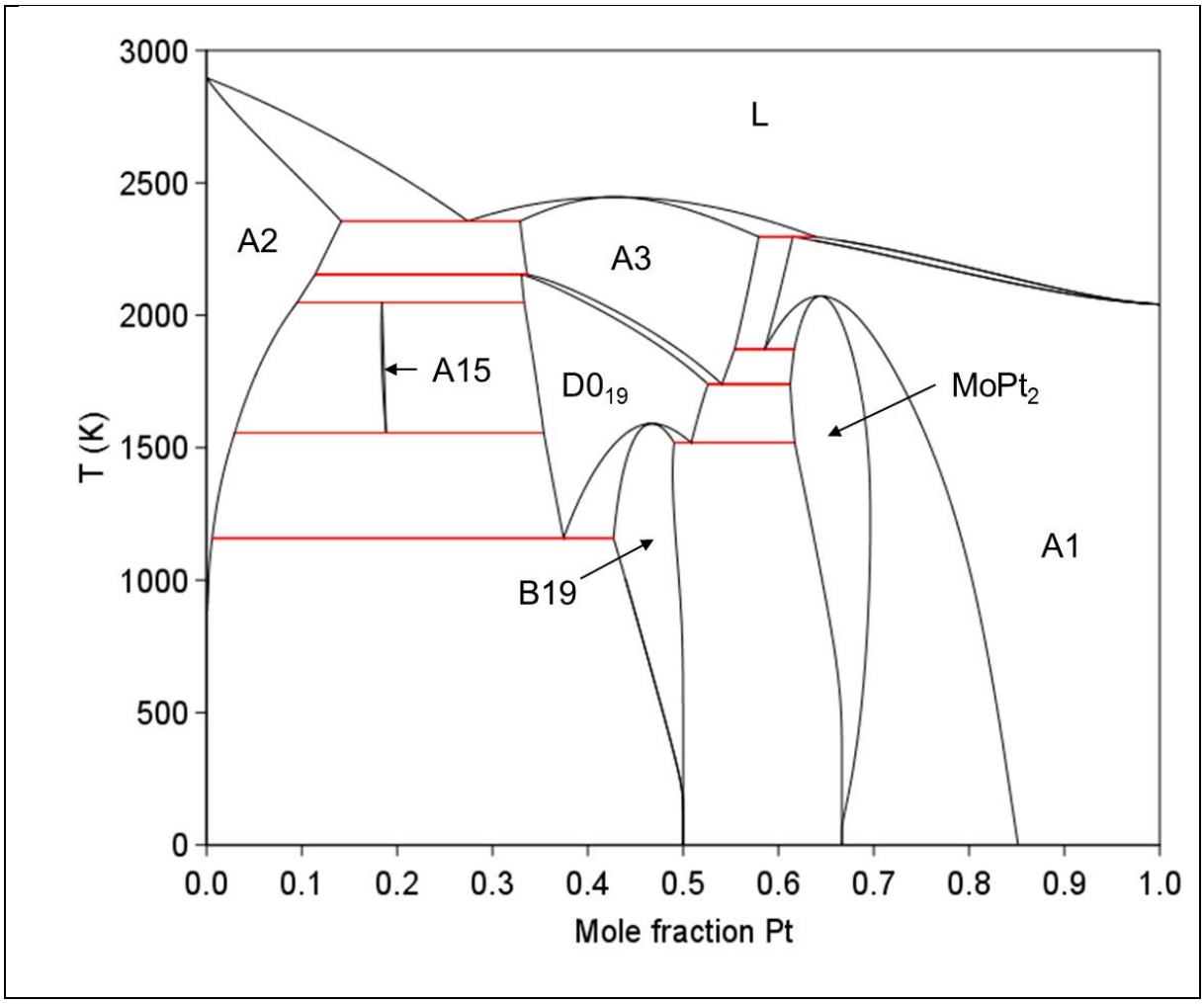

Fig. 3. The calculated Mo–Pt phase diagram from the current assessment.

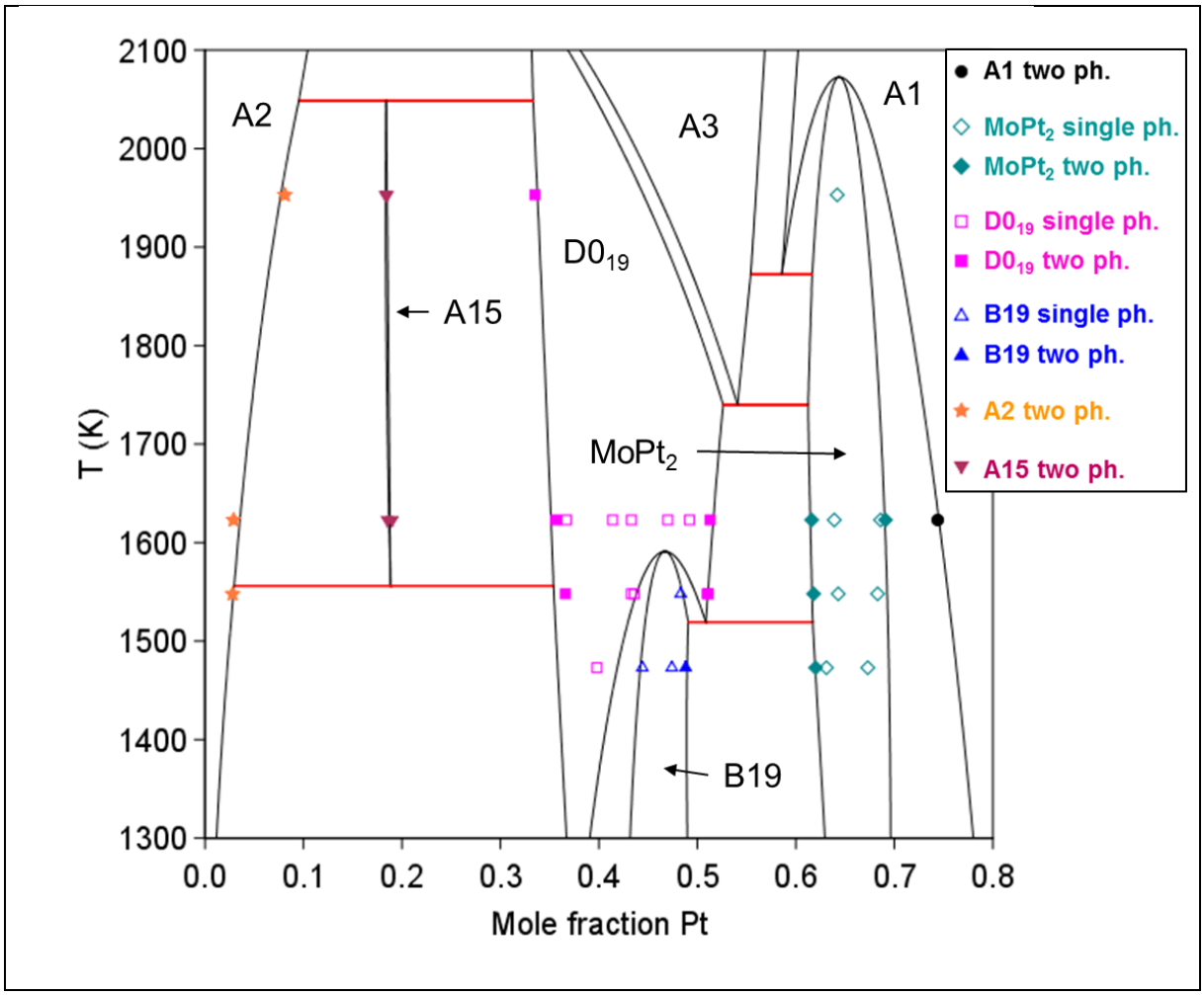

Fig. 4. Enlarged part of the calculated Mo-Pt phase diagram compared with experimental data from Ref. [8].

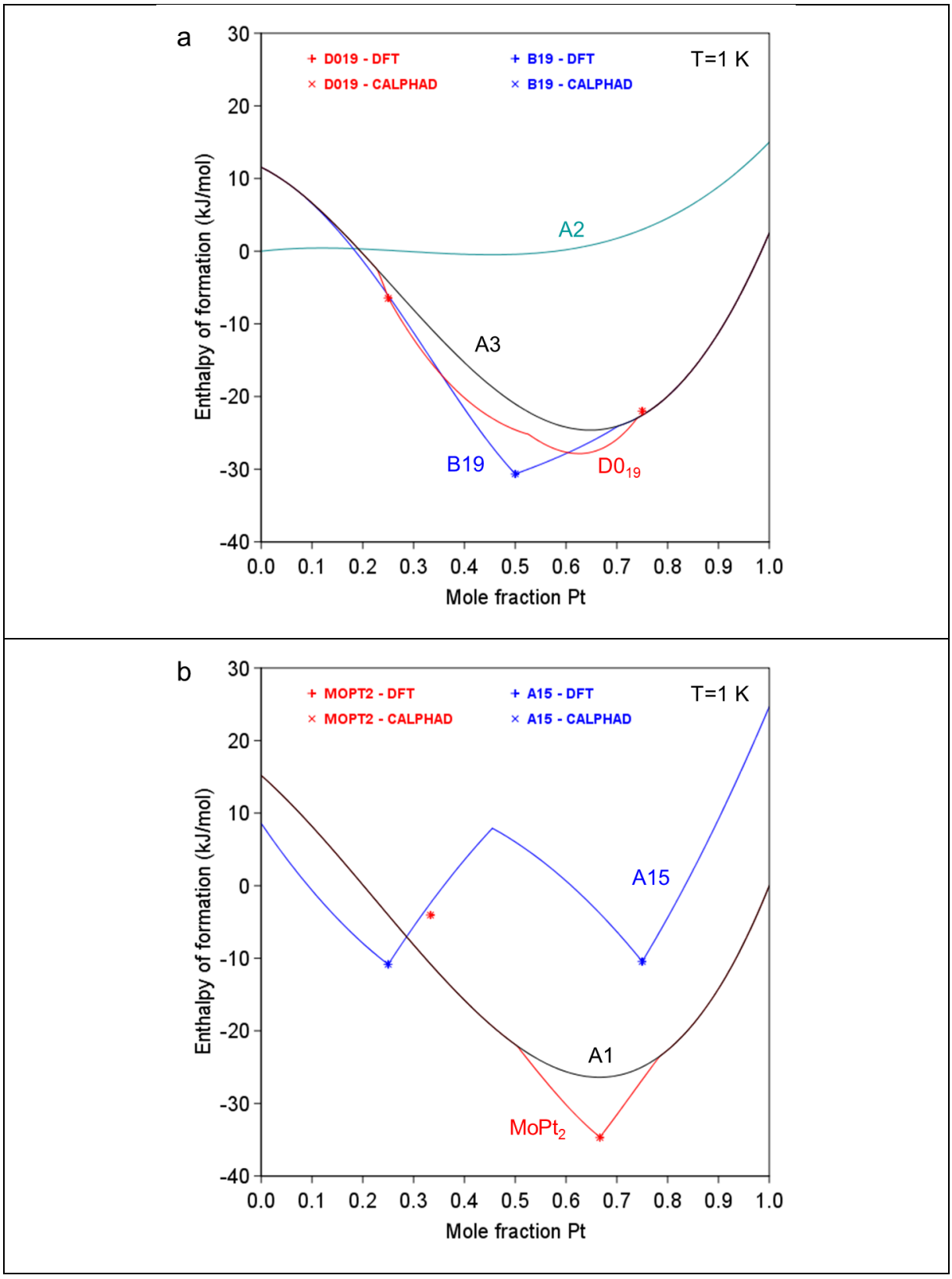

Fig. 5. Calculated enthalpies of formation at 1 K (lines) and compound energies at 0 K (symbols) obtained from FP and CALPHAD calculations (see Table 5) for the (a) *A*2, *A*3, *B*19, $D0_{19}$, (b) *A*1, *A*15 and $MoPt_2$ phases. Reference states are bcc Mo and fcc Pt.

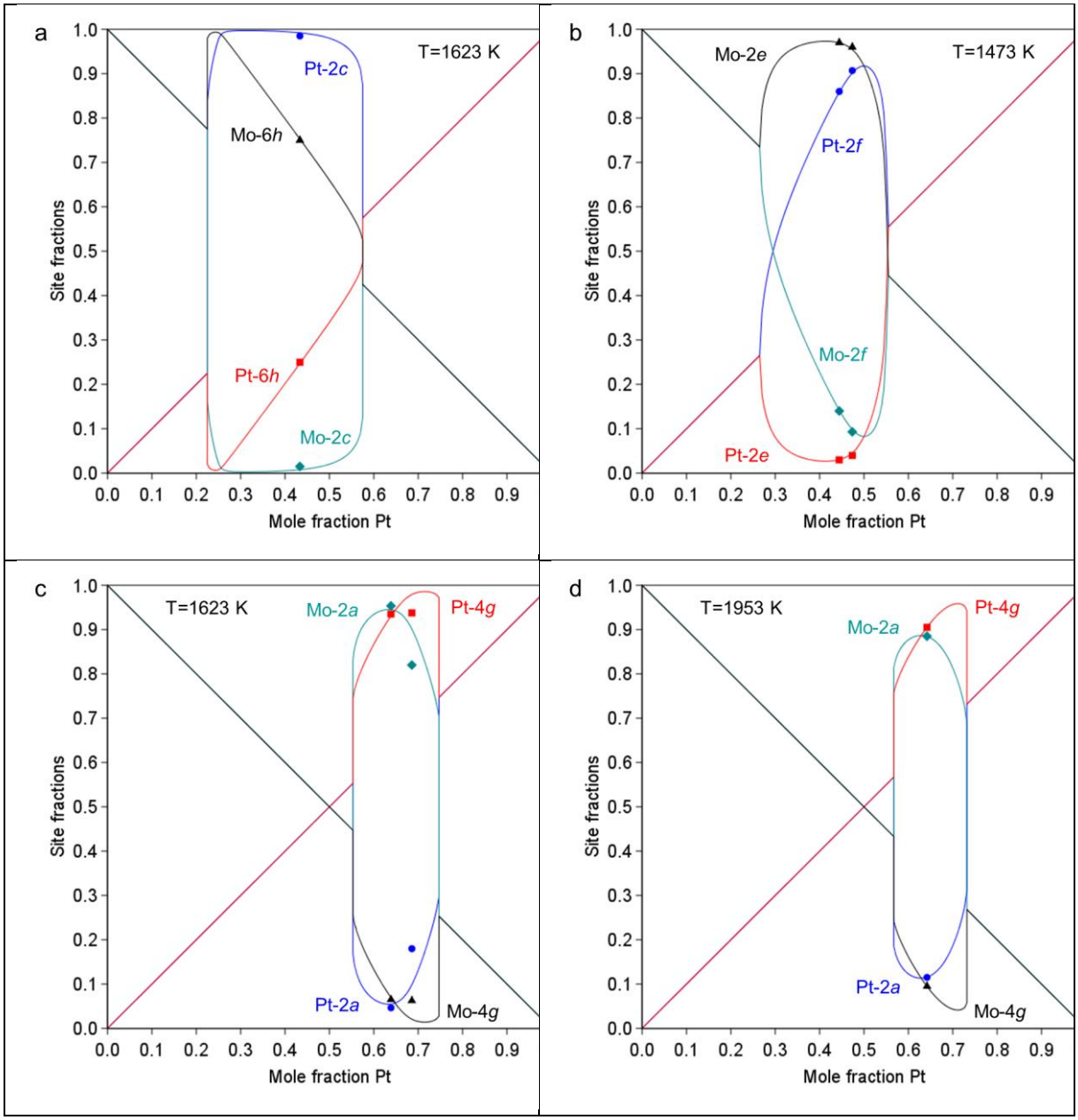

Fig. 6. Calculated site occupancies of the $D0_{19}$ (a), $B19$ (b) and $MoPt_2$ (c,d) phases. Corresponding experimental data from Ref. [8] are also plotted for comparison.